Model Predictive Control-enabled Fault Ride Through Operation Strategy for High Power Wind Turbine

Pedro Catalán[1], Yanbo Wang[2], Zhe Chen[2], Joseba Arza[3]

[1]*Ingeteam Power Technology S.A.,* Zamudio, Spain
[2]*AAU Energy, Aalborg University,* Aalborg, Denmark
[3]*Ingeteam R&D Europe,* Zamudio, Spain

E-mail: pedro.catalan@ingeteam.com, ywa@et.aau.dk, zch@et.aau.dk, joseba.arza@ingeteam.com

Keywords

«Model Predictive Control», «Wind energy», «Grid-connected converter», «Fault ride-through», «Converter control».

Abstract

The increasing penetration of wind power poses new requirements in terms of ancillary services to support the stable operation of power system. Based on the flexible positive and negative sequence control (FPNSC) method for current reference generation, this paper presents a model predictive control (MPC)-enabled fault ride through operation strategy for high power wind turbine complying with next-generation grid code requirements. The proposed strategy calculates the current references considering the converter current constraint, and further exploits the dynamic response of MPC to optimize the voltage support capability during balanced and unbalanced grid faults. Simulation results are given to validate the operation performance of the proposed fault ride through operation strategy.

Introduction

The offshore wind energy is promoting the penetration of wind power generation into power system. To exploit the offshore wind energy in a cost-effective way, the high-power wind turbine is being paid the increasing concerns. Consequently, the application of high-power Wind Energy Conversion System (WECS) has become an important trend in modern wind power system. The back-to-back neutral-point-clamped (NPC) converter [1]–[4] has been presented as an attractive option for high-power wind turbine in terms of power quality and system costs, which is able to perform medium voltage operation by three-level output.

Fault-ride through (FRT) operation capability of wind turbine is one of important concerns. The grid codes require that the wind turbine remains the uninterrupted grid-connected operation under a temporary voltage drop, where reactive power is injected into power grid to support voltage restoration. The requirements about reactive current injection are specified using voltage-time profiles. Also, the FRT operation must be accomplished within 20 ms once the grid voltage falls below the 90% value. In [5], the effect of current injection into power grid on transient stability is analyzed. The reactive power requirements have traditionally involved the positive sequence. However, in 2015 the German standard VDE-AR-N 4120 indicates the requirements for the negative sequence current injection for the first time [6]. In [7], the performance of a type-4 WT during unbalanced grid faults is analyzed, showing the positive effects of the negative current injection. According to the latest revisions from VDE, the next-generation grid codes will demand the injection of positive and negative-sequence reactive current in the presence of asymmetrical faults. Consequently, dual-sequence current reference control will be required. The Flexible Positive and Negative Sequence Control (FPNSC) is presented as a flexible structure in [8], which can accommodate different control objectives dependent on two independent gains for the reactive current injection in positive-sequence (k^+) and negative-sequence (k^-).

The advanced control strategies have been frequently developed for wind power converter. For instance, the application of finite control set model predictive control (FCS-MPC) in 3L-NPC converter has been paid increasing concerns [9]. In [10], the MPC of power converters applied in variable-speed WECS is reviewed. The application of FCS-MPC can improve the operation performance of wind power converters. In [11], a direct model predictive control scheme for NPC converter in permanent magnetic synchronous generator (PMSG)-based wind turbine for unbalanced grid is presented. In [12], a robust FCS-MPC control method for a direct-drive PMSG wind turbine system with NPC power converter is proposed. This work improves the robustness against parameter uncertainties by means of revised predictions of the state variables. In [13], a FCS model predictive direct torque and power control for 3L-NPC converter in PMSG-based wind turbine is developed. In [14], a model predictive direct power control for high-power NPC converters is presented. The instantaneous active and reactive power are regulated. In [15], a self-tuning FCS-MPC is proposed to control switching frequency of the 3L-NPC converter, which improves the power conversion efficiency. The method demonstrates its effectiveness against variations of grid impedance and the operating point.

However, the fault-ride through capability of NPC converter equipped with MPC in the presence of grid faults is merely addressed. Therefore, this paper presents an MPC-based control structure with FPNSC to operate with different reactive current injection profiles during grid faults. The effectiveness of the proposed control strategy is validated by simulation verification. Further, the capability of the 3L-NPC power converter to deal with both balanced and unbalanced voltage faults is investigated.

System Description

The 3L-NPC converter is widely used in high-power applications due to the good performance with low switching frequency. The aim of MPC is to regulate the currents into power grid according to the reference values. Also, the MPC is employed to regulate the neutral point potential of NPC converter, which are related with the switching state and converter currents. The outer control loops such as the grid synchronization and the DC-link voltage controller are adopted to generate the current references. Fig. 1 shows the diagram of 3L-NPC converter with FCS-MPC, where the discrete-time model is adopted to predict the future behaviors of the plant and implement the optimal control actions based on predefined control objectives.

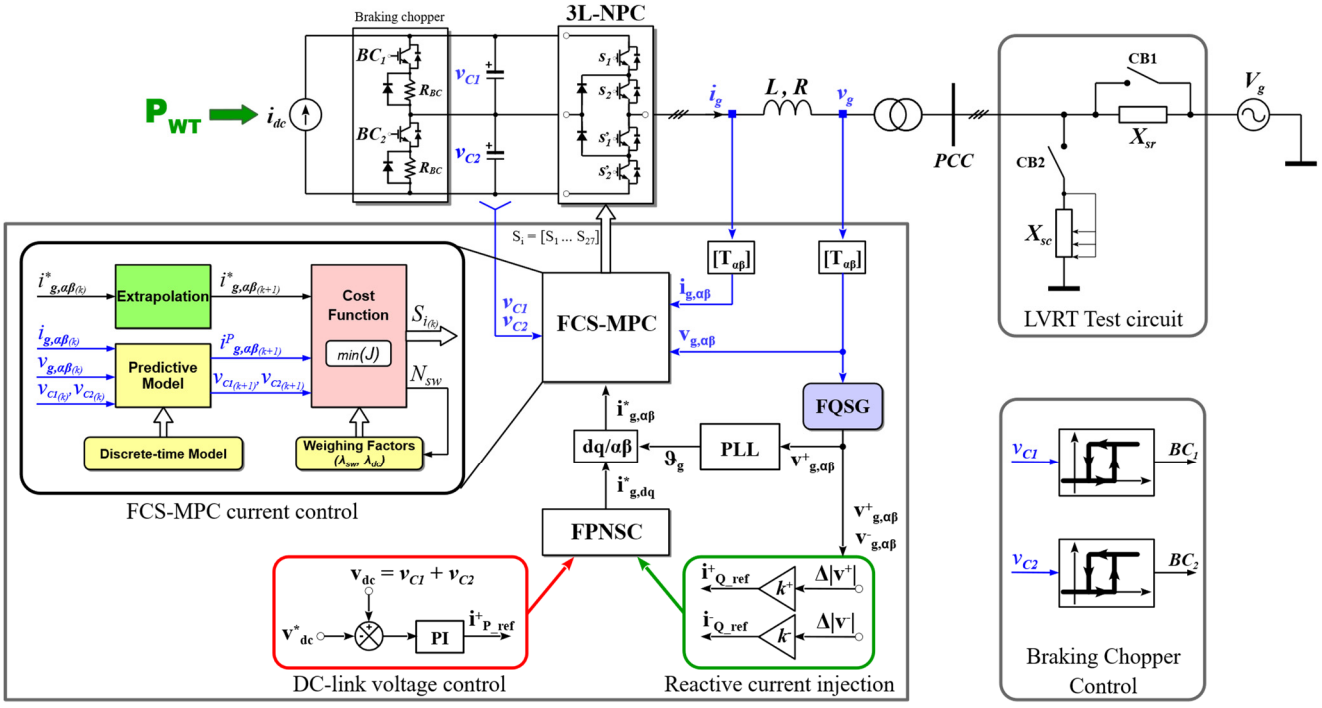

Fig. 1 The diagram of 3L-NPC converter with FCS-MPC.

The cost function considering the finite set of possible switching states of the power converter is established, where the given cost function is minimized by selecting the optimal state combination. Then, the optimal control law is obtained. The one-step horizon is proposed for the FCS-MPC. Although long prediction horizon usually leads to improved performance, it can be negligible for converters with an L-filter, whose transfer function is a first-order system. Moreover, long prediction horizons significantly increase the computational burdens, which affects the real-time implementation.

A. Operation Principle of Grid-Connected NPC Converter

The discrete-time model of injected grid current is established as (1).

$$i_{g(k+1)} = i_{g(k)} + \frac{T_s}{L}\left[v_{(k)} - Ri_{g(k)} - v_{g(k)}\right] \tag{1}$$

where R and L are the output resistance and inductance of the 3L-NPC converter, v is voltage generated by the converter, v_g is the grid voltage, T_s is the sampling time and i_g is the grid-injected current. The discrete model (1) is used to predict dynamic behaviors for the future value of grid current, considering all possible voltage vectors $\boldsymbol{v}$ generated by the NPC converter.

Currents in stationary reference frame can be controlled by defining a cost function based on the error between the predicted currents and the extrapolated references. To estimate the grid current error at (k+1) sampling instant, the reference currents are extrapolated to (k+1) state. The reference extrapolation technique can be used to compensate the sampling delay (T_s), and decrease the average reference tracking error [16].

$$J_i = \left(\left[i^*_{g,\alpha(k+1)} - i_{g,\alpha(k+1)}\right]^2 + \left[i^*_{g,\beta(k+1)} - i_{g,\beta(k+1)}\right]^2\right) \tag{2}$$

B. DC-link Voltage Balance of NPC Converter

The current through the clamping diodes and neutral point causes voltage imbalance between capacitors. When the output voltage is set to 0, the voltage of DC-link midpoint may fluctuate. Hence, a neutral point balancing control strategy is required to mitigate voltage imbalance. Considering NPC converter switching states, the discrete-time model of the DC-link capacitors is established as (3).

$$\begin{aligned} v_{C1(k+1)} &= v_{C1(k)} + \frac{T_s}{C_1} i_{C1(k)} \\ v_{C2(k+1)} &= v_{C2(k)} + \frac{T_s}{C_2} i_{C2(k)} \end{aligned} \tag{3}$$

where v_{C1}, v_{C2} and i_{C1}, i_{C2} are the voltages and currents in DC-link capacitors $C1$ and $C2$, respectively.

Currents through the capacitors are obtained based on the load currents and the present switching state. Thus, no additional measurements are required. The DC-link capacitors voltage balance is added to the cost function as a secondary goal J_{dc} as (4).

$$J_{dc} = \lambda_{dc} \cdot \left[v_{C1(k+1)} - v_{C2(k+1)}\right]^2 \tag{4}$$

where v_{C1} and v_{C2} are the voltages of DC-link capacitors and λ_{dc} is the weighting factor.

C. Switching Frequency Control

The absence of modulator in FCS-MPC results in random switching frequency. A new element J_{sw} is incorporated into cost function to reduce switching frequency by the simple penalty strategy [17].

$$\Delta s_i(k) = |s_i(k) - s_i(k-1)| \tag{5}$$

$$J_{sw} = \lambda_{sw} \cdot \frac{1}{N} \sum_{i=1}^{N} \Delta s_i(k)$$

where $s_i(k)$ is the state of each i switching element, N is the number of switching elements and λ_{sw} is the weighting factor.

The overall reduction of the switching frequency can be performed since the change of state is penalized, so that the controller is encouraged to remain in the same state. The reduction of switching frequency will decrease the switching losses, which improves the power conversion efficiency.

The cost function of the MPC controller is defined by combining the following control objectives. (1) the AC current tracking error in $\alpha\beta$-domain, (2) the DC-link neutral point balance, (3) the switching frequency by the simple penalty approach.

$$J = J_i + J_{dc} + J_{sw} \tag{6}$$

The proposed fault ride through operation strategy based on MPC

As described previously, both positive and negative-sequence currents need to be regulated in a dual-decoupled control framework. This includes injection of active power in the positive-sequence, injection of capacitive reactive power in the positive sequence to support positive-sequence voltage, and injection of inductive reactive power in negative sequence to attenuate negative-sequence voltage. To address this, a synchronization structure that may extract the positive sequence and negative sequence of grid voltage is needed. In this paper, the FQSG-PLL [18] is employed to estimate the voltage sequences and the MPC is used to regulate the grid currents in the αβ-frame.

This section presents the proposed strategy for generating the current references according to the FPNSC structure. First, the grid code requirements for reactive power injection are described. Second, the limiting values for the current references and the remaining capacity for active power are calculated considering the converter current constraint. Third, the operation of braking chopper to protect DC-link during grid faults is described. Finally, the dual-decoupled current references are referred to the αβ-frame to be regulated by the MPC.

A. Reactive Current Reference

In the presence of voltage fault events, the low-voltage ride-through requirements consider reactive current injection both in the positive-sequence and in the negative-sequence. The reactive current references needed for compliance are given as (7).

$$\begin{aligned} i_{Q\_ref}^{+} &= k^{+} \cdot \Delta|v^{+}| \\ i_{Q\_ref}^{-} &= k^{-} \cdot \Delta|v^{-}| \end{aligned} \tag{7}$$

where $i_{Q\_ref}^{+}$ is the positive-sequence reactive current reference, $i_{Q\_ref}^{-}$ is the negative-sequence reactive current reference, k^{+} and k^{-} are the gains applied to the grid voltage deviations $\Delta|v^{+}|$ and $\Delta|v^{-}|$. The proportional gains are defined by grid operators in the range of $0 \leq k \leq 6$, in order to optimize the grid voltage support capability.

B. Current Limitation

The selection of the current references should consider the converter current constraint I_{max}, which is determined by operating conditions such as cooling temperature, switching frequency or supported overload. The positive-sequence and the negative-sequence current references are defined within the current constraint of the power converter as (8) and (9).

$$|I^{+}| + |I^{-}| \leq I_{max} \tag{8}$$

$$|I^+| = \sqrt{\left(I^+_{P\_ref}\right)^2 + \left(I^+_{Q\_ref}\right)^2}$$
$$|I^-| = \sqrt{\left(I^-_{P\_ref}\right)^2 + \left(I^-_{Q\_ref}\right)^2} \quad (9)$$

where $|I^+|$ is the amplitude of the current reference in the positive sequence, defined by its components for active current ($I^+_{Q\_ref}$) and reactive current ($I^+_{Q\_ref}$), and $|I^-|$ is the amplitude of the current reference in the negative sequence, defined by its components for active current ($I^-_{P\_ref}$) and reactive current ($I^-_{Q\_ref}$).

If active current in negative sequence is set as zero ($I^-_{P\_ref}$ = 0), the equations (8) and (9) can be rewritten as (10).

$$\sqrt{\left(I^+_{P\_ref}\right)^2 + \left(I^+_{Q\_ref}\right)^2} + I^-_{Q\_ref} \leq I_{max} \quad (10)$$

The current references should be prioritized to satisfy converter current constraint. Considering that $I^+_{Q\_ref}$ and $I^-_{Q\_ref}$ are determined for grid-code compliance, the cascade-limits for current references are given as (11)-(13).

$$limI^-_Q = I_{max} \quad (11)$$

$$limI^+_Q = I_{max} - I^-_{Q\_ref} \quad (12)$$

$$limI^+_P = \sqrt{\left(I_{max} - I^-_{Q\_ref}\right)^2 - \left(I^+_{Q\_ref}\right)^2} \quad (13)$$

where $limI^-_Q$ is the limitation of the negative-sequence reactive current reference $I^-_{Q\_ref}$, $limI^+_Q$ is the limitation of the positive-sequence reactive current reference $I^+_{Q\_ref}$, and $limI^+_P$ is the limitation of the positive-sequence active current reference $I^+_{P\_ref}$.

C. DC-link voltage controller

The DC-link voltage controller generates the positive-sequence active current reference $I^+_{P\_ref}$ to regulate the active power output of the power converter.

In the presence of grid fault, the active power absorption capability of power grid is decreased. And reactive current is injected to support grid voltage restoration, which further reduces the limit for the active current reference as (13). Additionally, the active current injection is null during severe grid faults to avoid instability system. However, the mechanical system of wind turbine still maintains the active power injection in transient period. This power imbalance between the generated power and power injected to the grid should be dissipated by employing a braking chopper, which avoids the voltage boost in DC-link. In the NPC converter, each half bus is protected by a braking chopper as shown in Fig. 1.

The braking chopper is operated by the hysteresis control of the voltage at the capacitor terminals. Considering the nominal voltage V_{dc}, the chopper switch-on voltage is fixed at $V_{BC\_on} = 1.15\ V_{dc}$ and the switch-off voltage is fixed at $V_{BC\_off} = 1.05\ V_{dc}$. The switch-on voltage must ensure a safety margin with regards to the maximum working voltage of the components. Further, the voltage difference between both hysteresis thresholds must be sufficient to moderate the switching frequency. The braking resistor R_{BC} must be sized to dissipate rated active power, and its minimum value is established to keep the current value and the power losses of the braking semiconductor below the maximum ratings.

D. Current controller references

The MPC is responsible to regulate the grid currents in the αβ-frame. Then, the current references should be transferred from the dual-decoupled control framework to the αβ-frame by means of the positive-sequence voltage angle ϑ_g ($v^+_q \approx 0$) defined by the FQSG-PLL as (14)-(16).

$$i_{\alpha}^{*} = i_{\alpha\_ref}^{+} + i_{\alpha\_ref}^{-}$$
$$i_{\beta}^{*} = i_{\beta\_ref}^{+} + i_{\beta\_ref}^{-} \quad (14)$$

$$i_{\alpha\_ref}^{+} = \frac{v_d^{+}}{|v^{+}|} i_{P\_ref}^{+} \cdot \cos\vartheta_g + \frac{v_d^{+}}{|v^{+}|} i_{Q\_ref}^{+} \cdot \sin\vartheta_g$$
$$i_{\beta\_ref}^{+} = \frac{v_d^{+}}{|v^{+}|} i_{P\_ref}^{+} \cdot \sin\vartheta_g - \frac{v_d^{+}}{|v^{+}|} i_{Q\_ref}^{+} \cdot \cos\vartheta_g \quad (15)$$

$$i_{\alpha\_ref}^{-} = \frac{-v_q^{-}}{|v^{-}|} i_{Q\_ref}^{-} \cdot \cos\vartheta_g + \frac{v_d^{-}}{|v^{-}|} i_{Q\_ref}^{-} \cdot \sin\vartheta_g$$
$$i_{\beta\_ref}^{-} = \frac{v_q^{-}}{|v^{-}|} i_{Q\_ref}^{-} \cdot \sin\vartheta_g + \frac{v_d^{-}}{|v^{-}|} i_{Q\_ref}^{-} \cdot \cos\vartheta_g \quad (16)$$

where $i_{\alpha\_ref}^{+}$ and $i_{\beta\_ref}^{+}$ are the αβ-frame representation for the positive-sequence current references, $i_{\alpha\_ref}^{-}$ and $i_{\beta\_ref}^{-}$ are the αβ-frame representation for the negative-sequence current references, and i_{α}^{*} and i_{β}^{*} are the αβ-frame current references for the predictive controller. v_d^{+}, v_d^{-} and v_q^{-} are the grid voltage components obtained from the FQSG-PLL.

Simulation Verification

In this section, time-domain simulation in MATLAB/SIMULINK is performed to validate the proposed fault-ride through operation strategy for 3L-NPC converter in the presence of grid faults. The detailed parameters of the system are given in Table I.

TABLE I: SIMULATION PARAMETERS

Parameter	Value
Rated Power P_N	4 MW
LV Rated Voltage V_g	3100 V
HV Rated Voltage V_{HV}	66000 V
DC-link voltage V_{dc}	5600 V
Switching frequency f_{sw}	1 kHz
DC-link capacitors C_1, C_2	20 mF
Braking chopper resistor R_{BC}	1.0 Ω
Filter Inductance L	400 µH
Filter Resistor R	1.3 mΩ
Sampling Time T_s	50 µs

A. Test system description

Fig. 1 shows the FRT Test circuit in simulation verification. The FRT test system is designed based on the following aspects. (1) the rapid generation of two- or three-phase voltage dips at the instant of the fault can be performed, (2) the constant voltage during the fault duration at a reduced LVRT value can be produced, (3) the rapid voltage recovery to the original voltage value at the instant of fault clearing can be performed.

The variable series reactance (*Xsr*) is used to limit the short circuit current, so that only a small reduction in voltage at the grid side is observed during a fault simulation. The short circuit reactance (*Xsc*) is used to obtain the required voltage dip. The short circuit reactance is variable, so that dips with various magnitudes of the applied voltage can be obtained. The series reactance circuit breaker (*CB1*) is used to bypass the series reactance (*Xsr*) during normal operation of the power converter. The circuit

breaker is opened at 1s before the introduction of the short circuit and closed sometime after the short circuit is removed. The short circuit breaker (*CB2*) is used to generate and end the time-controlled voltage dips.

B. Simulation results analysis

The power converter is operated at rated active power in steady state. The simulation tests include 100% voltage faults at PCC at 2s. The active power input to the DC-link remains unchanged during the whole test. All of the results are obtained from a post-processing of the voltages and currents measured at PCC to extract the positive and negative sequence.

Fig. 2 shows the simulation results of 3L-NPC converter system during a 3-phase 100% voltage fault at PCC. In Fig. 2 (a), the reactive current injection profile has been configured as $k^+ = 0$ and $k^- = 0$, which implies that positive-sequence reactive current is set as zero. In Fig. 2(b), the reactive current injection profile has been specified as $k^+ = 2$ and $k^- = 0$, which implies that positive-sequence reactive current will reach rated values for those voltage faults over 50%. In both cases, the negative-sequence reactive current is null since the voltage fault is balanced.

Fig. 3 shows the simulation results of 3L-NPC converter system during a 100% 2-phase voltage fault at PCC. In Fig. 3 (a), the reactive current injection profile has been specified as $k^+ = 2$ and $k^- = 0$, which implies that negative-sequence reactive current is set as zero. In this case, due to the lack of negative-sequence current injection, the power converter can be operated with active current because of the current limit remainder. The minor effect is caused by the fact that the voltage fault has been directly generated at PCC. In Fig. 3(b), the reactive current injection profile has been specified as $k^+ = 2$ and $k^- = 2$. In this case, both positive- and negative-sequence reactive current are injected into the grid. The current imbalance slightly reduces the voltage imbalance.

The simulation results show the quick dynamic response of the MPC-based current controller can be implemented since the reactive current is injected within less than 20ms. Additionally, the stable operation of the power converter during the fault events has been demonstrated. The power imbalance between the generated power and power injected to the grid is dissipated by the braking chopper, which maintains the voltage boost under safety margins. After the fault clearance, the active current returns to its original value in a ramped manner to continue the steady state operation.

Conclusion

This paper presents an MPC-based fault ride through operation strategy for 3L-NPC converter applied in high-power wind turbine. The FPNSC method is proposed to generate current references, and the limiting values are derived according to converter current constraint. The FCS-MPC is used to regulate the currents into the power grid in the αβ-frame, to balance the neutral point potential, and to control the switching frequency of NPC converter. Furthermore, the dynamic response of MPC is exploited to optimize the voltage support capability during balanced and unbalanced grid faults. The operation performance of the proposed strategy is analyzed and validated against symmetrical and asymmetrical faults. The effectiveness of the MPC-based control strategy is validated for high-power wind converter operation during grid faults, which is applicable for modern grid code requirements of offshore wind power system.

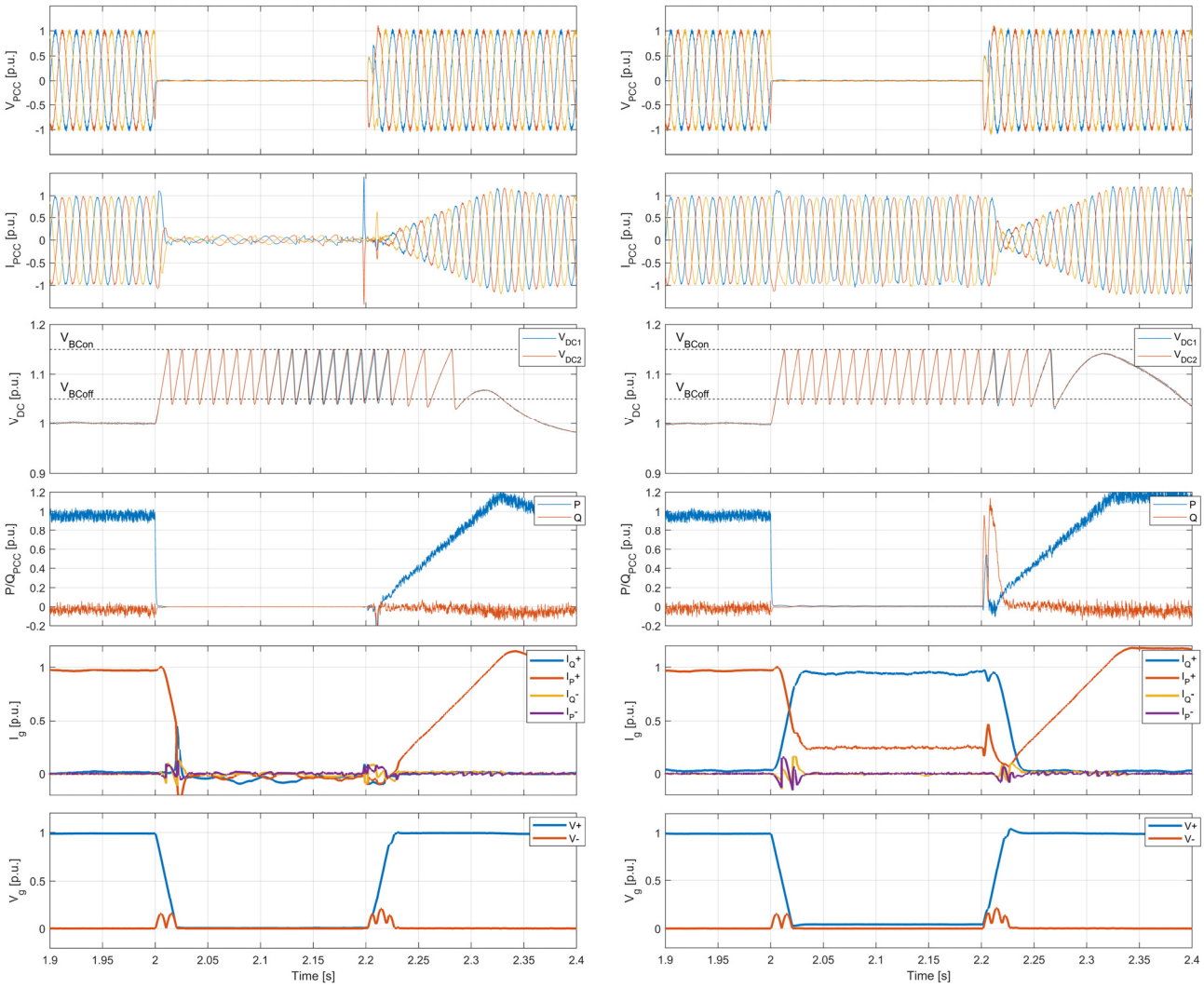

(a) (b)

Fig. 2 The simulation results of the 3L-NPC converter under balanced grid fault.
(a) $k^+ = 0$, $k^- = 0$, (b) $k^+ = 2$, $k^- = 0$.

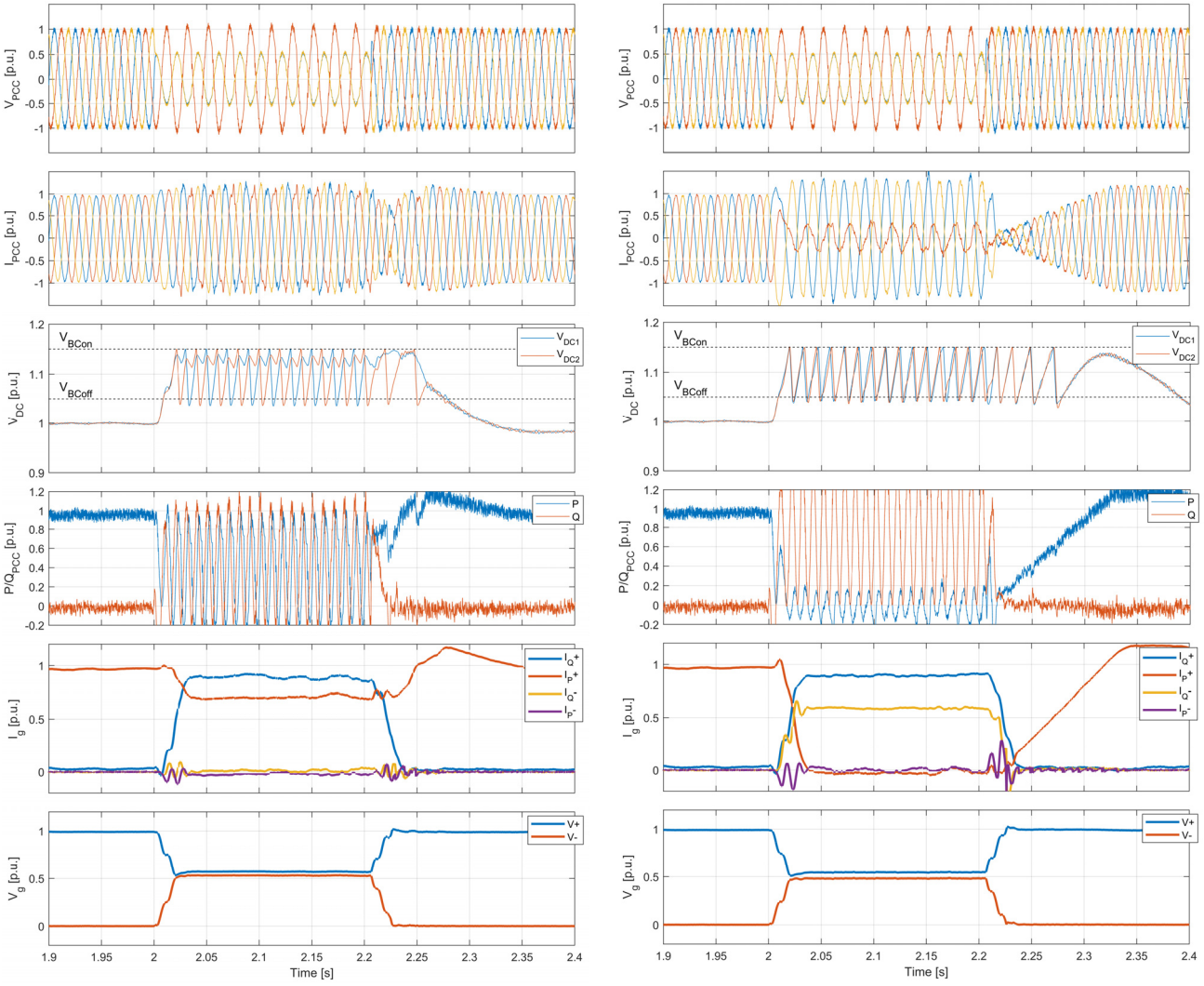

Fig. 3 The simulation results of the 3L-NPC converter under unbalanced grid fault.
(a) $k^+ = 2$, $k^- = 0$, (b) $k^+ = 2$, $k^- = 2$.

References

[1] A. Nabae, I. Takahashi, and H. Akagi, "A New Neutral-Point-Clamped PWM Inverter," *IEEE Trans. on Ind. Applicat.*, vol. IA-17, no. 5, pp. 518–523, Sep. 1981.

[2] J. Rodriguez, S. Bernet, P. K. Steimer, and I. E. Lizama, "A Survey on Neutral-Point-Clamped Inverters," *IEEE Trans. Ind. Electron.*, vol. 57, no. 7, pp. 2219–2230, Jul. 2010.

[3] J. Chivite-Zabalza, I. Larrazabal, I. Zubimendi, S. Aurtenetxea, and M. Zabaleta, "Multi-megawatt wind turbine converter configurations suitable for off-shore applications, combining 3-L NPC PEBBs," in *2013 IEEE Energy Conversion Congress and Exposition*, Denver, CO, USA, 2013, pp. 2635–2640.

[4] J. Li, Z. Hu, Y. Wang, and Z. Chen, "H14 Three-Level Inverter for Common-Mode Voltage Suppression," *IEEJ Trans. Elec Electron. Eng.*, vol. 16, no. 2, pp. 315–323, Feb. 2021.

[5] I. Erlich, F. Shewarega, S. Engelhardt, J. Kretschmann, J. Fortmann, and F. Koch, "Effect of wind turbine output current during faults on grid voltage and the transient stability of wind parks," in *2009 IEEE Power & Energy Society General Meeting*, Calgary, Canada, 2009, pp. 1–8.

[6] VDE-AR-N 4120, “Technical requirements for the connection and operation of customer installations to the high voltage network (TAB high voltage),” Jan. 2015.

[7] T. Neumann, T. Wijnhoven, G. Deconinck, and I. Erlich, “Enhanced Dynamic Voltage Control of Type 4 Wind Turbines During Unbalanced Grid Faults,” *IEEE Trans. Energy Convers.*, vol. 30, no. 4, pp. 1650–1659, Dec. 2015.

[8] M. Graungaard Taul, X. Wang, P. Davari, and F. Blaabjerg, “Current Reference Generation Based on Next-Generation Grid Code Requirements of Grid-Tied Converters During Asymmetrical Faults,” *IEEE J. Emerg. Sel. Topics Power Electron.*, vol. 8, no. 4, pp. 3784–3797, Dec. 2020.

[9] J. Rodriguez *et al.*, “State of the Art of Finite Control Set Model Predictive Control in Power Electronics,” *IEEE Trans. Ind. Inf.*, vol. 9, no. 2, pp. 1003–1016, May 2013.

[10] V. Yaramasu and B. Wu, *Model predictive control of wind energy conversion systems*. New York: Wiley, 2017.

[11] Z. Zhang and R. Kennel, “Direct Model Predictive Control of three-level NPC back-to-back power converter PMSG wind turbine systems under unbalanced grid,” in *2015 IEEE International Symposium on Predictive Control of Electrical Drives and Power Electronics (PRECEDE)*, Valparaiso, 2015, pp. 97–102.

[12] Z. Zhang, Z. Li, M. P. Kazmierkowski, J. Rodriguez, and R. Kennel, “Robust Predictive Control of Three-Level NPC Back-to-Back Power Converter PMSG Wind Turbine Systems with Revised Predictions,” *IEEE Trans. Power Electron.*, vol. 33, no. 11, pp. 9588–9598, Nov. 2018.

[13] Z. Zhang, F. Wang, J. Wang, J. Rodriguez, and R. Kennel, “Nonlinear Direct Control for Three-Level NPC Back-to-Back Converter PMSG Wind Turbine Systems: Experimental Assessment With FPGA,” *IEEE Trans. Ind. Inf.*, vol. 13, no. 3, pp. 1172–1183, Jun. 2017.

[14] J. Scoltock, T. Geyer, and U. K. Madawala, “Model Predictive Direct Power Control for Grid-Connected NPC Converters,” *IEEE Trans. Ind. Electron.*, vol. 62, no. 9, pp. 5319–5328, Sep. 2015.

[15] P. Catalan, Y. Wang, Z. Chen, and J. Arza, “Model Predictive Control Strategy for NPC Converter-based Wind Turbine with Switching Frequency Control,” in *2021 IEEE Southern Power Electronics Conference (SPEC)*, Kigali, Rwanda, 2021, pp. 1–7.

[16] P. Cortes, F. Quiroz, and J. Rodriguez, “Predictive control of a grid-connected cascaded H-bridge multilevel converter,” in *Proceedings of the 2011 14th European Conference on Power Electronics and Applications*, 2011, pp. 1–7.

[17] R. Vargas, P. Cortes, U. Ammann, J. Rodriguez, and J. Pontt, “Predictive Control of a Three-Phase Neutral-Point-Clamped Inverter,” *IEEE Trans. Ind. Electron.*, vol. 54, no. 5, pp. 2697–2705, Oct. 2007.

[18] J. I. Garcia, J. I. Candela, A. Luna, and P. Catalan, “Grid synchronization structure for wind converters under grid fault conditions,” in *IECON 2016 - 42nd Annual Conference of the IEEE Industrial Electronics Society*, Florence, Italy, 2016, pp. 2313–2318.